Paper No.
19066

AMPP ANNUAL CONFERENCE + EXPO
MARCH 19-23, 2023 | DENVER, COLORADO

Influence of Impurity Adsorption and Condensation on the Initial Corrosion Mechanism of CO_2 Transport Pipeline Steel

Minghe Xu
State Key Laboratory of Power Systems, Department of Thermal Engineering, Tsinghua University, Beijing, 100084, P.R. China.

Yoon-Seok Choi, Srdjan Nesic
Institute for Corrosion and Multiphase Technology,
Department of Chemical and Biomolecular Engineering, Ohio University
342 West State Street
Athens, OH 45701
USA

ABSTRACT

The present study was designed to study the role of impurity adsorption and condensation behaviors in the corrosion mechanism of CO_2 transport pipeline steel, based on the hypothesis that the impurity adsorption and condensation play a critical role in inducing the formation of aqueous electrolyte in the initial stage of the corrosion processes. The impurity adsorption and condensation behaviors including water adsorption, adsorption of sulfurous species (SO_2/H_2SO_3), and H_2SO_3 condensation onto the Fe-coated quartz crystals were measured by the Quartz Crystal Microbalance (QCM) technique in water-unsaturated CO_2/H_2O flow and CO_2/H_2O/H_2SO_3/SO_2 flow at 45°C and 1 bar. The connections between the water adsorption and acid condensation behavior onto Fe-coated quartz crystals with Fe corrosion were also studied by utilizing SEM and EDS techniques. The results showed that Fe suffered no corrosion in the water-unsaturated CO_2/H_2O gas flow but suffered localized corrosion in the water-unsaturated CO_2/H_2O/H_2SO_3/SO_2 gas flow. It was suggested that the acid condensation initiated the Fe corrosion at water-unsaturated conditions with impurities instead of the pure water adsorption behavior.

Key words: Carbon Capture and Storage, CO_2 corrosion, carbon steel, SO_2, acid condensation

INTRODUCTION

CO_2 captured from different sources for carbon capture and storage (CCS) will contain impurities. Although it is technologically possible to treat CO_2 to near 100% purity in the gas conditioning process, it is preferable to have fewer rigid specifications to reduce both operational and capital costs. From a corrosion point of view, SO_x, NO_x, H_2S, and O_2 are considered to be the most aggressive impurities. There are no field cases that analyzed the effect of impurities on corrosion,

however, laboratory experiments have shown that noticeable, and potentially severe, corrosion occurs at water-unsaturated conditions in dense phase CO_2 with the presence of those impurities due to synergistic interactions between chemical species.[1-11]

Although many experimental works have been conducted to investigate the effects of water and various impurities on the corrosion behavior of pipeline steels in dense phase CO_2, there is little study on the evaluation of corrosion mechanisms for the corrosion behavior of pipeline steels in dense phase CO_2, especially for the corrosion mechanism in the water-unsaturated conditions.

The corrosion process for carbon steel exposed to wet CO_2 mainly consist of three stages: the initial stage for the electrolyte formation, the intermediate stage for the chemical and electrochemical reactions that occur both on the steel-electrolyte interface and in the bulk phase, and the final stage for the nucleation and growth of the corrosion products. For the corrosion mechanism at the water-unsaturated conditions with dense phase CO_2, the initial corrosion mechanisms play the most important role in initiating the corrosion process and determining the extent of general corrosion and localized corrosion. However, it remained unknown that how the electrolyte formed and how corrosion was initiated at water-unsaturated conditions in dense phase CO_2 with impurities, in which case the free water phase was not supposed to exist.

There are four possible explanations for the initial corrosion mechanism from the literature.[12-17] The first explanation argued that the impurities (SO_2, O_2, NO_2, etc.) could decrease the water solubility in the dense phase CO_2,[12] thus inducing the water condensation onto the steel surface. However, the existing studies showed that small amounts of impurities could not significantly decrease the water solubility. Take O_2 as an example,[13] it was reported that the presence of 2.5 mol.% O_2 in CO_2 lowered the actual water solubility limit by approximately 100 ppm_v at 38°C, 12 MPa, comparing with the theoretical water solubility in pure CO_2. The decreased water solubility is not large enough to induce the water condensation when the water amount is far below the theoretical water solubility. The second explanation argued that because the temperature and pressure might vary during the operation processes, especially in the field,[14] the water solubility in the CO_2 phase would change with the temperature and pressure, thus the water condensation would occur. Dugstad et. al.,[15] also pointed out in some applications, when the liquid or supercritical CO_2 leaked out, the pressure would drop and induce the water condensation. The above two explanations focused on how water condensation could occur when the water contents are below the theoretical water solubility in the CO_2 phase at the theoretical conditions, and the motivation for water condensation is the change of actual water solubility, which either derived from the impact of impurities or the change of environments. However, these two explanations could be used as the possible reasons, but not the general reasons for the electrolyte formation at the water-unsaturated conditions. The third explanation argued that it was the water adsorption and accumulation at the pipeline steel-CO_2 interface that induced the electrolyte formation due to the hydrophilic nature of the steel surface.[16] But it remains doubt as to whether the amount of adsorbed and accumulated water is sufficient to initiate corrosion. The fourth explanation is proposed herein that the electrolyte formation at the water-unsaturated conditions in the CO_2 with acid gas impurities is derived from the acid condensation,[17] and the evaluation of this hypothesis is the focus of the present work.

In order to investigate the initial corrosion mechanism, this work was designed to study the role of impurity adsorption and condensation behavior in CO_2 corrosion mechanism, based on the hypothesis that the impurity adsorption and condensation play a critical role in inducing the formation of aqueous electrolyte in the initial corrosion stage for the CO_2 corrosion processes at water-unsaturated conditions. Before stepping into the high pressure CO_2 conditions, this work mainly addressed with the corrosion at the low pressure in 1 bar CO_2 gas flow. It was suggested

that there are some similarities for the corrosion mechanisms between the low pressure CO_2 conditions and high pressure CO_2 conditions including characteristics of CO_2 corrosion product scale and the variation rule of corrosion rate with temperature.[18]

EXPERIMENTAL PROCEDURE

Quartz Crystal Microbalance

In the present work, Fe-coated quartz crystal of 5 MHz resonant frequency with 1.37 cm^2 of effective area was used (Figure 1 (a)). The Fe-coated quartz crystal was selected to investigate the connections between the water and impurity adsorption with corrosion initiation.

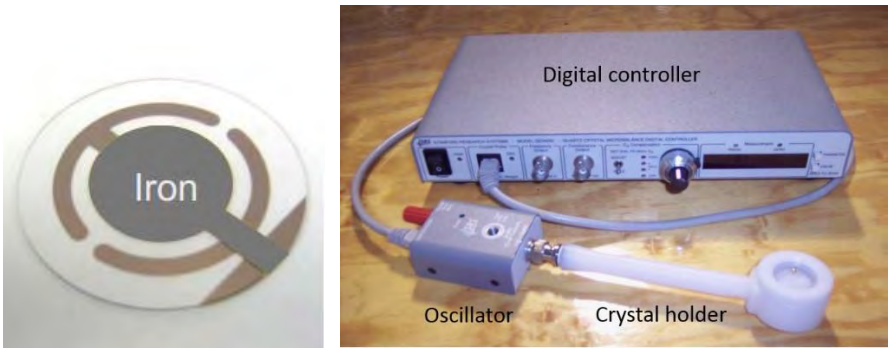

(a) (b)

Figure 1: Images of quartz crystals and Quartz Crystal Microbalance (QCM) system: (a) Fe-coated quartz crystal, (b) Quartz Crystal Microbalance (QCM)

A sensitive QCM technique, which can yield a mass sensitivity of 10^{-9} g/cm^2 and detect a mass change in nano gram scale, has been widely used to study adsorption, condensation, and deposition processes, because of its economical, usable and reliable characteristics.[19,20] QCM is an acoustic-wave sensor in which the acoustic wave propagates in the direction perpendicular to the quartz crystal surfaces. The basic principle behind all acoustic-wave sensors is that adding mass on the quartz crystal surface of the sensor causes the resonant frequency to decrease.[21] Thus, QCM technique is utilized to measure the mass change per unit area by measuring the change in frequency of a quartz crystal. The mass change on the Fe-coated surfaces of the resonator due to the resonant frequency change in the gas phase is given by the Sauerbrey equation:[22]

$$\Delta f = -C_f \cdot \Delta m \quad (1)$$

where Δf is the frequency change (Hz), C_f is the sensitivity factor for the quartz crystal (56.6 Hz $\mu g^{-1} cm^2$ for a 5 MHz AT-cut quartz crystal), and Δm is the change in mass per unit area ($g \cdot cm^{-2}$).

Experimental Set-up for Water Adsorption Tests

A 2 L glass cell containing deionized water was used as a water bath to control the temperature of the QCM chamber at 45.0 ± 0.1°C. The QCM chamber with 200 ml volume acted as a confined space, where water and impurity could adsorb onto the quartz crystal surface. Figure 2 shows a schematic diagram of the experimental set-up for the water adsorption tests using QCM. It mainly consisted of a CO_2 gas cylinder and gas lines, a saturator, QCM chamber, and humidity

measurement device. After the dry CO_2 gas left the cylinder, the gas flow rate was kept constant at around 40 mL/min for each test.

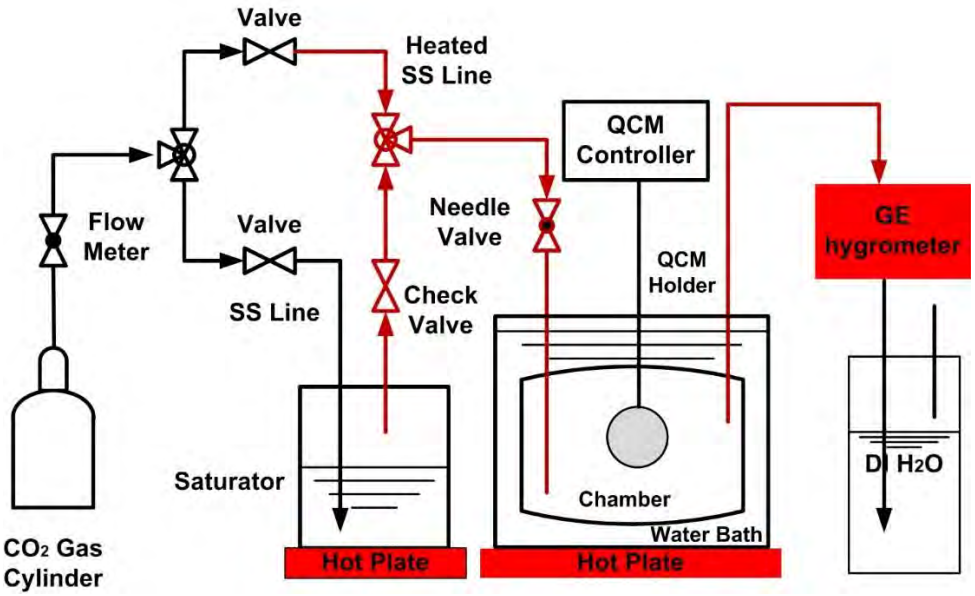

Figure 2: The Experimental Set-up for Water Adsorption Tests with the Fe-coated quartz crystals.

Once the gas source was opened, the dry CO_2 gas either passed through the dry gas line into the QCM chamber or passed through the saturator to be saturated with water vapor. The dry and wet gas paths were controlled by a three-way valve. The dry CO_2 gas was used to remove the moisture inside the QCM chamber before conducting the test, while the wet CO_2 gas was used to conduct the water adsorption tests. After the wet gas mixture left the saturator, it passed through the heated stainless steel gas lines and entered the QCM chamber. The stainless steel gas lines were heated to above 50°C to minimize the moisture loss along the gas paths due to the potential water condensation, which might derive from the temperature differences between the gas mixture and gas lines.

The water-unsaturated CO_2 gas flow with various relative humidities was generated by utilizing the two-temperature difference method. By bubbling CO_2 in the saturator, which contained deionized water at the temperature of T_s, the water vapor with saturated vapor pressure at T_s was added into the CO_2 gas flow. Afterwards, the wet CO_2 gas flowed from the saturator into the QCM chamber at higher temperature (T_b) of 45°C, thus the CO_2 gas flow became water-unsaturated ($T_s < T_b$). The relative humidity (RH) of the CO_2 gas flow was calculated by the division of the saturated water vapor pressure at T_s to the saturated water vapor pressure at T_b (Equation 2). T_s ranged from 9°C to 40°C, while T_b was kept constant at 45°C, thus the relative humidity in CO_2/H_2O gas flow ranged from 10% to 75%.

$$RH\ (\%) = \frac{p_{sat}(T_s)}{p_{sat}(T_b)} \times 100 \quad (2)$$

where p_{sat} (T) represents the saturated vapor pressure of water at temperature of T (°C) and can be calculated by Equation 3:

$$p_{sat}(T) = 10^{A-B/(C+T)} \quad (3)$$

where A, B, C represent Antoine Constants for Water. When water temperature is in the range of 1 to 100°C, A = 8.07131, B = 1730.63, C = 233.426.[23]

The relative humidity was also measured by using a humidity measurement device in the gas downstream. The device was a microprocessor-based, single-channel hygrometer that measured moisture content in gases, and it was suitable for a wide range of process conditions requiring real-time moisture measurement. The measured relative humidity was usually ± 5% difference from the calculated relative humidity, which implied that the measured relative humidity showed a good match with the calculated relative humidity.

Experimental Set-up for the Adsorption and Condensation of Sulfurous Species Tests

The experimental set-up for the sulfurous species (H_2SO_3/SO_2) tests was basically identical to that for the water adsorption tests, except that 6% w/v H_2SO_3 solution was added into the saturator instead of the deionized water. In this way, the 1 bar CO_2 flow would be contaminated by the impurities of $H_2O(g)$, $SO_2(g)$ and $H_2SO_3(g)$ when it passed through the saturator to turn into $CO_2/H_2O/SO_2/H_2SO_3$ gas flow. Since H_2SO_3 solution was volatile acid, $SO_2(g)$ would be generated by the decomposition of H_2SO_3, according to the Equation 4:

$$H_2SO_{3(l)} \leftrightarrow SO_{2(g)} + H_2O_{(l)} \quad (4)$$

It is worthy to mention that $H_2SO_3(g)$ probably existed in the CO_2 gas mixture because stable $H_2SO_3(g)$ in the gas phase was once detected by Sulzle et al.[23]

Since the relative humidity sensor in the humidity measurement device was easily corroded by the sulfurous species, the hygrometer was removed from the set-up. Thus, T_s was respectively set as 32°C and 38°C, while T_b was kept constant at 45°C, thus the relative humidity of 45% and 70% in $CO_2/H_2O/SO_2/H_2SO_3$ gas flow was respectively achieved in the QCM chamber. As a H_2SO_3 solution rather than pure water is used, the actual values of humidity may differ from the calculated results. Therefore, experiments were conducted on 45% and 70%, which can show a sufficient difference. For the tail gas treatment, $NaHCO_3$ aqueous solution was used to absorb the gas mixture to prevent the SO_2 pollution.

Surface analysis

Apart from the QCM technique, scanning electron microscopy (SEM) and energy-dispersive X-ray spectroscopy (EDS) were employed to investigate the corrosion initiation on the Fe-coated quartz crystals. Before and after the Fe-coated quartz crystals were exposed to the CO_2/H_2O and $CO_2/H_2O/SO_2/H_2SO_3$ gas flow, the SEM technique was used to observe the crystal surface morphology to examine whether corrosion was initiated and furthermore to study the corrosion products morphology once corrosion did occur. EDS technique was also used to detect the elemental composition of the crystal surfaces before and after the QCM tests.

RESULTS

Test Results for Fe-coated Quartz Crystal Exposed to CO_2/H_2O gas flow

The water adsorption behavior onto the Fe-coated quartz crystals was measured upon exposure to the water-unsaturated CO_2/H_2O gas flow with various humidities. The series of water adsorption

tests was repeated twice with the QCM technique and the results for the amounts of adsorbed water onto the Fe-coated quartz crystals are shown in Figure 3.

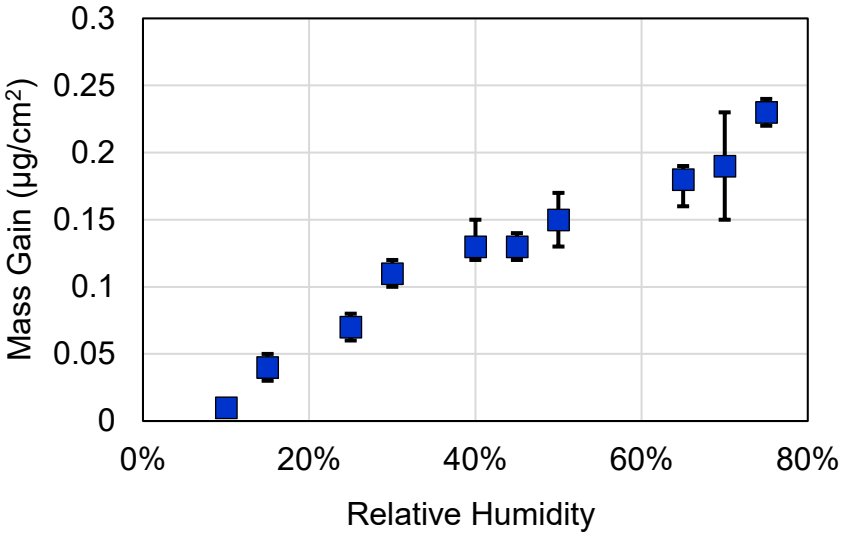

Figure 3: Mass gain on the Fe-coated quartz crystals exposed to CO_2/H_2O gas flow at 45.0°C, 1 bar under different humidities.

The mass gain on the Fe-coated quartz crystals generally increased from 0.01 µg/cm^2 to 0.23 µg/cm^2 with the relative humidity was increased from 10% to 75%. Furthermore, the adsorbed water first increased steeply from 0.01 to 0.11 µg/cm^2 with the relative humidity increasing from 10% to 30%, then leveled out between 0.11 and 0.13 µg/cm^2 with the relative humidity increasing from 30% to 45%, afterwards increased gradually from 0.15 to 0.23 µg/cm^2 with the relative humidity increasing from 50% to 75%. The general shape of the water adsorption curve onto Fe surfaces is typical for the water adsorption to hydrophilic surfaces.[24]

By assuming that the adsorbed water was uniformly distributed on the surface, and the adsorbed water was monolayer mode instead of bilayer mode,[25] the number of equivalent monolayers of water on Fe was calculated and shown in Table 1, based on the estimation that 0.01 µg/cm^2 is corresponding to 1 water monolayer.[26] The estimated thickness of adsorbed water layer was at nanometer (nm) scale, which was quite not easily perceived.

Little literature data on the use of QCM for adsorption of water on Fe were found. However, Lee et al.'s study[27] showed similar results with the current research and the authors also utilized the QCM method to investigate the water adsorption behavior on the iron in the conditions of humidified air at the temperatures of 7 ~ 85°C. They indicated that the amounts of adsorbed water on Fe at 45°C in the humidified air with the relative humidity of 20%, 50% and 95% were 0.1 µg/cm^2, 0.15 µg/cm^2, and 0.28 µg/cm^2, respectively. The measured amounts of adsorbed water on Fe at 45°C in the current research and Lee et al.'s study were similar, which suggested that the water adsorption behavior might not be highly affected by the mainstream (CO_2 or air), and furthermore confirmed the credibility of the QCM method.

Table 1
Estimated equivalent number of water monolayer adsorbed on Fe-coated quartz crystals exposed to CO_2/H_2O gas flow with various relative humidity.

Relative Humidity / %	Equivalent Number of Water Monolayers in Current Work	Thickness of Water Layers
10%	1-2	0.2-0.4 nm
15%	4-5	0.8-2 nm
25%	7-8	1.4-3.2 nm
30%	11-12	2.2-4.8 nm
40%	13-14	2.6-5.6 nm
45%	13-14	2.6-5.6 nm
50%	15-16	3.0-6.4 nm
65%	18-19	3.6-7.6 nm
70%	19-20	3.8-8.0 nm
75%	22-23	4.4-9.2 nm

In order to test whether corrosion occurred on the Fe-coated quartz crystals in CO_2/H_2O gas flow, the QCM tests were performed at the relative humidity of 45% and 70%. For each relative humidity, the tests were repeated by three times. Before and after being exposed to the CO_2/H_2O flow, the Fe-coated quartz crystals were examined by SEM and EDS techniques to detect whether corrosion was initiated. As shown in Figure 3, the amounts of gained masses for the Fe-coated quartz crystals upon exposure to CO_2/H_2O gas flow were 0.13 ± 0.01 μg/cm^2 and 0.19 ± 0.04 μg/cm^2 at the relative humidity of 45% and 70%, respectively. The SEM images and EDS results for the Fe-coated quartz crystals before and after the test in CO_2/H_2O gas flow are shown in Figure 4 and Table 2, respectively. Before the tests at the relative humidity of 45% and 70%, the surfaces of the Fe-coated quartz crystals were observed to be extremely smooth by SEM, and mainly consisted of Fe elements. After the exposure to the CO_2/H_2O gas flow at 45.0°C, the morphology of the surfaces for the contaminated Fe-coated quartz crystals stayed very similar to the fresh surfaces, and so did the elemental composition. Thus, it was concluded that there was no corrosion at the relative humidity of 45% and 70%. This confirms that the mass gains for the Fe-coated quartz crystals were dominantly derived from the water adsorption onto the Fe-coated quartz crystals instead of the multiple effects (water adsorption + corrosion).

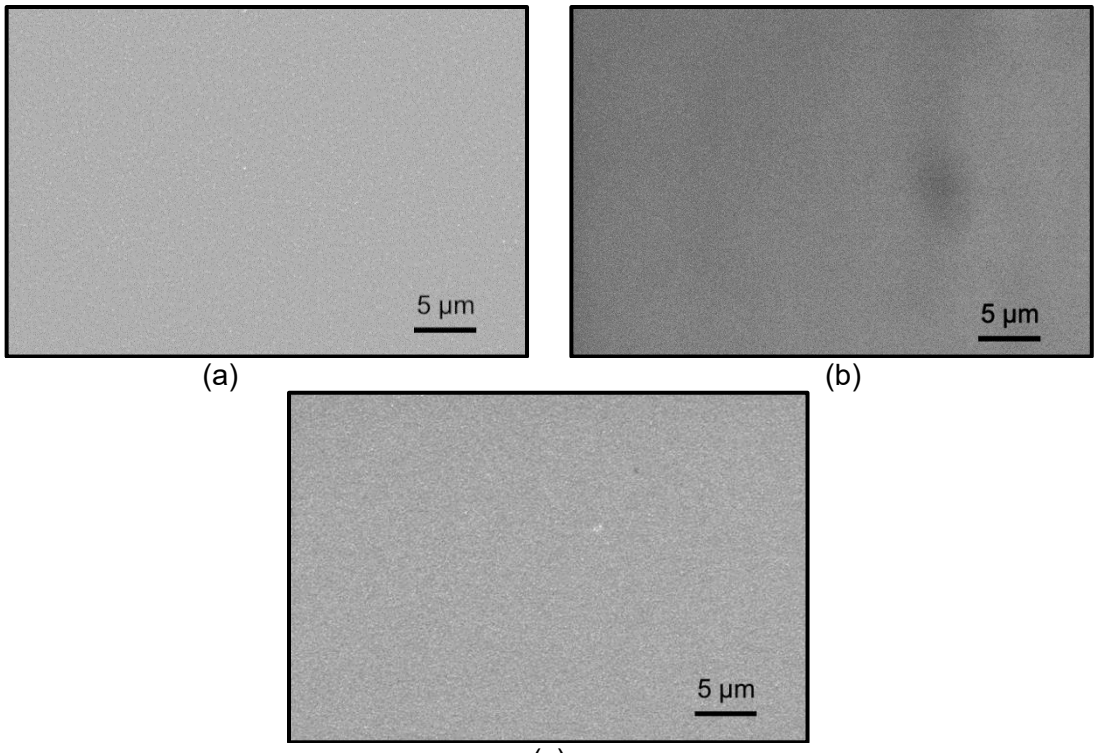

Figure 4: SEM images of the Fe-coated quartz crystals before and after being exposed to CO_2/H_2O gas flow at 45.0°C, 1 bar: (a) Before test, (b) After test (45% RH), (c) After test (70% RH).

Table 2
EDS results for the Fe-coated quartz crystals before and after exposure to CO_2/H_2O gas flow.

Element (Atom %)	Fe	C	O
Before test	95.97	2.08	1.98
After test (45% RH)	96.2	2.03	1.78
After test (70% RH)	95.17	2.73	2.10

Test Results for Fe-coated Quartz Crystal Exposed to $CO_2/H_2O/SO_2/H_2SO_3$ gas flow

The real-time mass change for the Fe-coated quartz crystal exposed to $CO_2/H_2O/SO_2/H_2SO_3$ gas flow for 24 hours at the relative humidity of 45% is shown in Figure 5. The adding mass onto the quartz crystal kept increasing for the first 10 hours, while stayed relatively constant at about 7.5 µg/cm^2 afterwards. From the amount of mass gain, which was tens of times higher than the amounts of mass gain in the CO_2/H_2O gas flow, it was suggested that corrosion could occur. Corrosion products on the Fe-coated quartz crystal were also observed with naked eye during the test. Besides, the SEM images for the Fe-coated quartz crystal after exposure to the CO_2 gas mixtures (Figure 6) illustrates that the corrosion products locally grew on the surface. The EDS analysis (Table 3) showed that the corrosion products were mainly composed of Fe, S, O and C elements (regions B and D in Figure 6), while the areas between the corrosion products were

mainly composed of Fe (regions A and C in Figure 6), which suggested that the overall surface suffered localized corrosion.

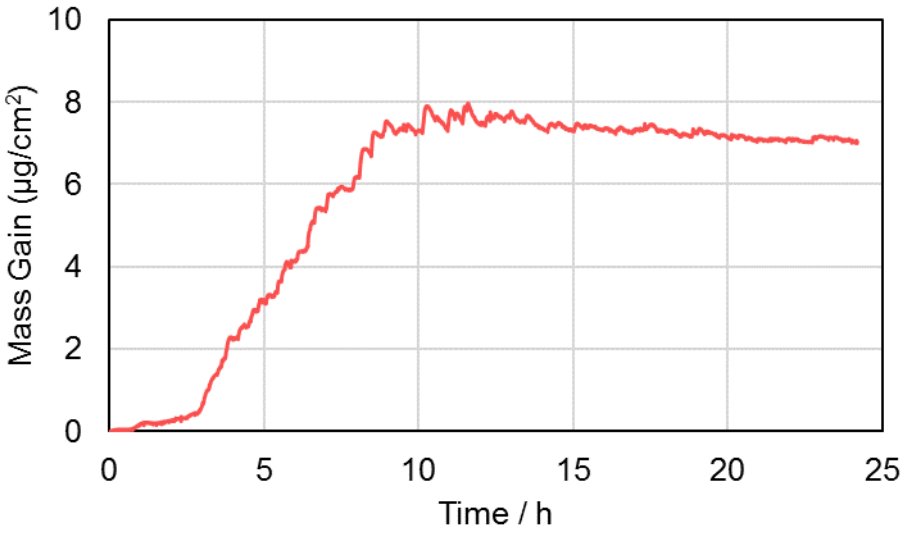

Figure 5: Mass change curve with time for the Fe-coated quartz crystal exposed to $CO_2/H_2O/SO_2/H_2SO_3$ gas flow for 24 hours at 1 bar, 45°C with 45% relative humidity.

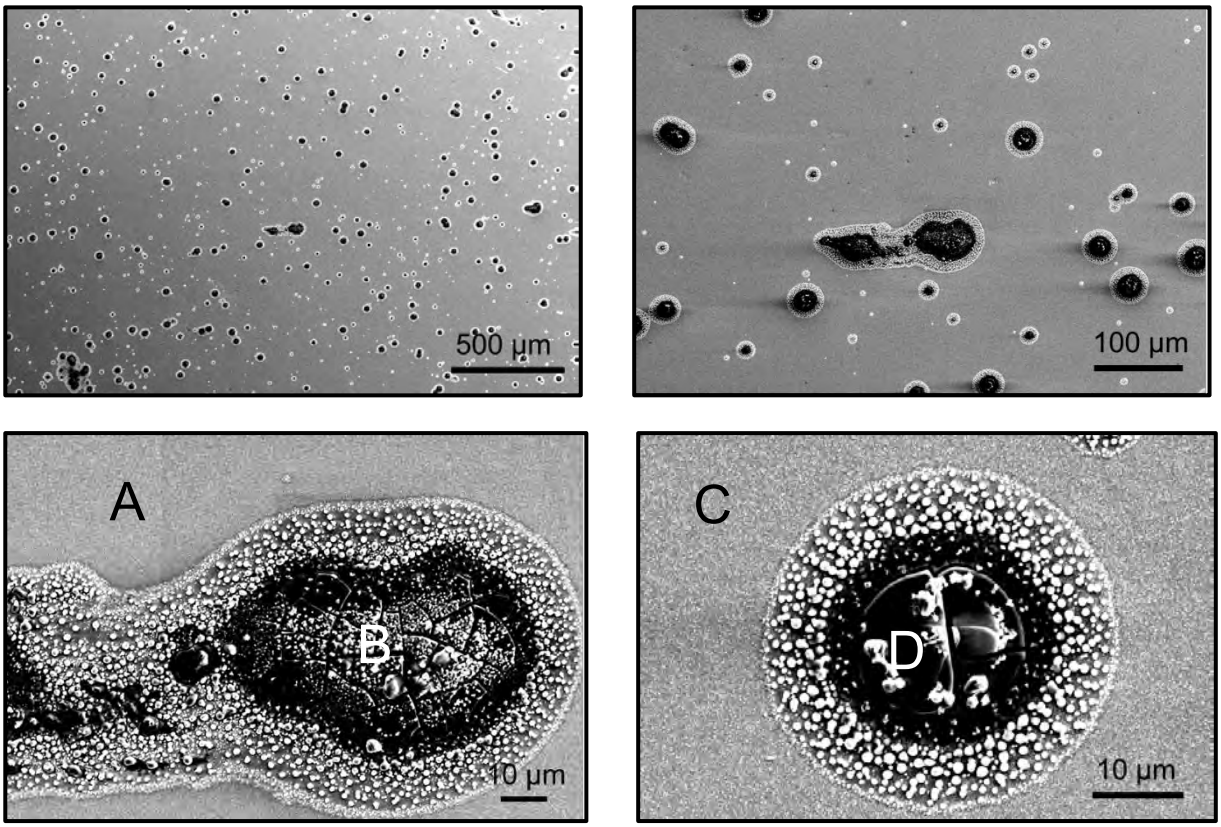

Figure 6: SEM images for the Fe-coated quartz crystals after being exposed to $CO_2/H_2O/SO_2/H_2SO_3$ gas flow with 45% relative humidity at 45.0°C, 1 bar.

Table 3
EDS results for Regions A-D in Figure 6 that showed the SEM images for the Fe-coated quartz crystals after exposure to $CO_2/H_2O/SO_2/H_2SO_3$ gas flow

Element (Atom %)	Fe	C	O	S
Region A	96.37	2.05	1.59	--
Region B	43.64	14.58	21.75	20.04
Region C	96.62	1.73	1.65	--
Region D	42.37	11.32	23.53	22.79

The real-time mass change for the Fe-coated quartz crystal exposed to $CO_2/H_2O/SO_2/H_2SO_3$ gas flow for 10 hours at the relative humidity of 70% is shown in Figure 7. The adding mass onto the quartz crystal kept increasing during the 10-hour exposure. Corrosion occurred under expectation as corrosion products were observed with naked eye. Again, the SEM images for the Fe-coated quartz crystal after exposure to the CO_2 gas mixtures also confirmed the corrosion phenomenon (Figure 8). The surface was also locally covered by the corrosion products which were generally in the fried-egg shape. In similar with the results obtained at the relative humidity of 45%, the EDS results in Table 4 indicate that the corroded products were mainly composed of Fe, S, O and C elements, while the gaps between the corrosion products were mainly composed of Fe.

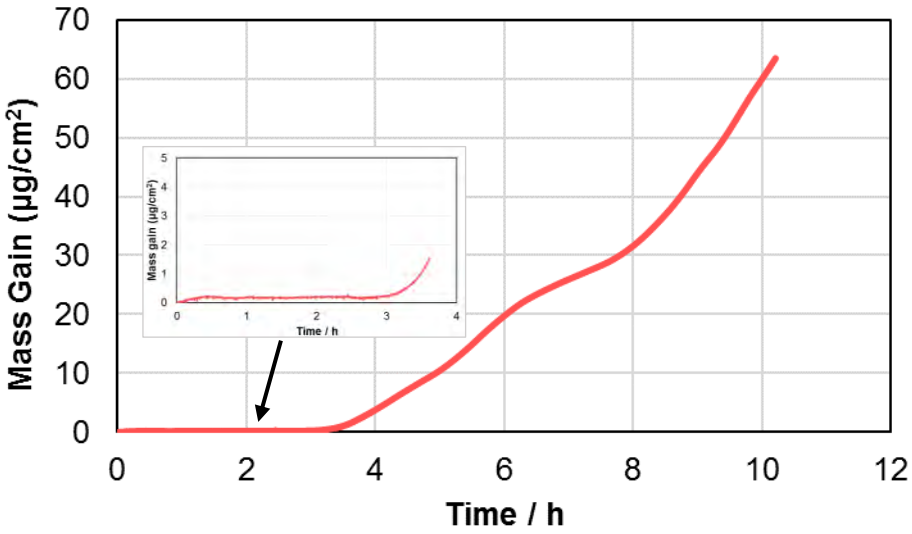

Figure 7: Mass change curve with time for the Fe-coated quartz crystal exposed to $CO_2/H_2O/SO_2/H_2SO_3$ gas flow for 10 hours at 1 bar, 45°C with 70% relative humidity.

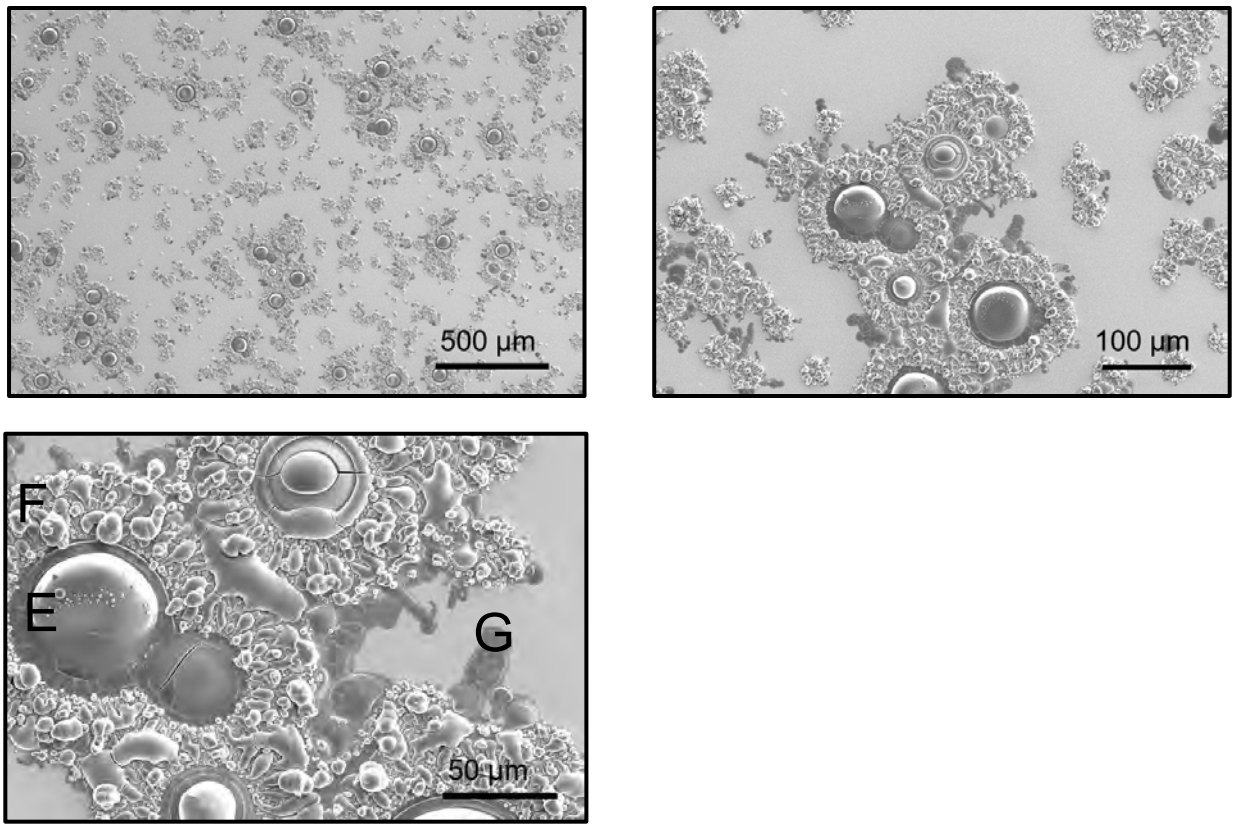

Figure 8: SEM images of the Fe-coated quartz crystals after being exposed to $CO_2/H_2O/SO_2/H_2SO_3$ gas flow with 70% relative humidity at 45.0°C, 1 bar.

Table 4
EDS results for Regions E-G in Figure 8 that showed the SEM images for the Fe-coated quartz crystals after exposure to $CO_2/H_2O/SO_2/H_2SO_3$ gas flow.

Element (Atom %)	Fe	C	O	S
Region E	35.19	10.03	40.09	14.69
Region F	64.39	6.53	16.23	12.86
Region G	96.27	1.65	2.09	--

DISCUSSION

The results showed that no corrosion for Fe-coated quartz crystals in the water-unsaturated CO_2/H_2O gas flow, while it suffered corrosion in the water-unsaturated $CO_2/H_2O/H_2SO_3/SO_2$ gas flow. Moreover, in the conditions that Fe-coated quartz crystals were exposed to $CO_2/H_2O/H_2SO_3/SO_2$ gas flow, the morphology of the corroded surfaces indicated that it was the localized corrosion with the island-pattern products instead of general corrosion (Figure 6 and Figure 8).

Since both CO_2/H_2O and $CO_2/H_2O/H_2SO_3/SO_2$ gas flow contained unsaturated water vapor, water adsorption would occur onto the Fe surface instead of water condensation behavior. In the tests with CO_2/H_2O gas flow, the adsorbed water was confirmed to incapably initiate the corrosion. In the tests with $CO_2/H_2O/H_2SO_3/SO_2$ gas flow, if the adsorbed water on the surface absorbed the SO_2 gas and H_2SO_3 gas, the aqueous phase would become acid and intended to corrode the iron. However, this explanation

for the corrosion initiation could not explain why only localized corrosion with the island-pattern products occurred. Another explanation suggested that it was the H_2SO_3 gas adsorption that initiated the corrosion, while it still could not explain why it was localized corrosion but not the general corrosion, unless the adsorption behavior was localized but not universal. Therefore, it is postulated that H_2SO_3 acid condensation dominated the corrosion initiation. The H_2SO_3 gas in the $CO_2/H_2O/H_2SO_3/SO_2$ gas flow either came from the evaporation of the H_2SO_3 solution in the upstream saturator or from the combination of $H_2O_{(g)}$ and $SO_{2(g)}$ in the gas flow. The H_2SO_3 acid condensation would occur when the temperature was at or below the acid dew point, which is calculated by Equation 5:[28,29]

$$1000/T_{dp} = 3.9526 - 0.1863\log_e(p_{H_2O}) + 0.000867\log_e(p_{SO_2})\ 0.000913\log_e(p_{H_2O})\log_e(p_{SO_2}) \quad (5)$$

where T_{dp} is the acid dew point temperature for the H_2SO_3 acid, in kelvins and p is the partial pressure, in mmHg. Since the H_2SO_3/SO_2 gas generation in the saturator is a dynamic process, it is difficult to predict the dynamic concentration for H_2SO_3 and SO_2. Therefore, the maximum H_2SO_3/SO_2 gas concentration in the gas mixtures at atmospheric pressure is estimated to be about 0.4 mol.% using Henry's Law under the assumption of the equilibrium state. Thus, the minimum acid dew point for H_2SO_3 acid is estimated to be about 40°C. The actual H_2SO_3 dew point temperature could be higher than the QCM chamber temperature of 45°C, if the H_2SO_3/SO_2 gas concentration is lower than 0.4 mol.% which could be the case during the experiments. Consequently, the H_2SO_3 acid can be condensed onto the iron surface and induced the corrosion.

The speculation for the initial corrosion mechanism can be expressed as follows:

$$SO_{2(g)} + H_2O_{(g)} \leftrightarrow H_2SO_{3(g)} \quad (6)$$

$$H_2SO_{3(g)} \rightarrow H_2SO_{3(aq)} \quad (7)$$

After the condensed H_2SO_3 formed on the Fe-coated quartz crystals, the corrosion occurred:

$$Fe_{(s)} + H_2SO_{3(aq)} \rightarrow FeSO_{3(s)} + H_{2(g)} \quad (8)$$

It is confirmed from the present study that the pure water adsorption behavior did not induce the electrolyte formation and the subsequent Fe dissolution in CO_2/H_2O flow at 1 bar and 45.0°C. Moreover, it is postulated that the corrosion of Fe was initiated by the H_2SO_3 acid condensation in $CO_2/H_2O/H_2SO_3/SO_2$ flow at 1 bar and 45.0°C. This work revealed the role of acid condensation in CO_2 corrosion mechanism at atmospheric pressure, and also inspired acid condensation to act as the initial electrolyte formation for the corrosion mechanism in dense phase CO_2 environments.

CONCLUSIONS

The impurity adsorption and condensation behavior including water adsorption, adsorption of sulfurous species (SO_2/H_2SO_3), and H_2SO_3 condensation onto Fe-coated quartz crystals in water-unsaturated CO_2/H_2O flow and $CO_2/H_2O/H_2SO_3/SO_2$ flow at 45°C, 1 bar was measured by the QCM technique. The connections between the water adsorption and acid condensation behavior onto Fe-coated quartz crystals with Fe corrosion were also studied. The conclusions are as follows:

- The Fe-coated quartz crystal showed no corrosion when it was exposed to the water-unsaturated CO_2/H_2O gas flow at 45°C, 1 bar although water adsorption occurred on the Fe-coated quartz crystals. The amounts of the adsorbed water on the Fe-coated quartz crystals ranged from 0.01 to 0.23 μg/cm^2 with the relative humidity varying from 10% to 75%.
- The Fe-coated quartz crystal suffered corrosion when it was exposed to the $CO_2/H_2O/SO_2/H_2SO_3$ gas flow at 45°C, 1 bar with the relative humidities of 45% and 70%. The initial corrosion

mechanism was postulated to be derived from the H_2SO_3 condensation from the point of view of the morphology for the corroded surfaces.

- The investigation of the initial corrosion mechanism for CO_2 corrosion at atmospheric pressure provided the implication that the H_2SO_3, H_2SO_4 and HNO_3 acid condensation could potentially induce the pipeline steel corrosion in the dense phase CO_2 mixtures with unsaturated water.

REFERENCES

1. Y. Hua, R. Barker, A. Neville, "The Effect of O_2 Content on the Corrosion Behaviour of X65 and 5Cr in Water-Containing Supercritical CO_2 Environments," *Applied Surface Science* 356 (2015): p. 499.
2. Y. Hua, R. Barker, A. Neville, "The Influence of SO_2 on the Tolerable Water Content to Avoid Pipeline Corrosion During the Transportation of Supercritical CO_2," *International Journal of Greenhouse Gas Control* 37 (2015): p. 412.
3. M. Xu, W. Li, Y. Zhou, X. X. Yang, Z. Wang, Z. Li, "Effect of Pressure on Corrosion Behavior of X60, X65, X70, and X80 Carbon Steels in Water-Unsaturated Supercritical CO_2 Environments," *International Journal of Greenhouse Gas Control* 51 (2016): p. 357.
4. A. Dugstad, M. Halseid, ""Internal Corrosion in Dense Phase CO2 Transport Pipelines—State of the Art and the Need for Further R&D," CORROSION 2012, paper no. 0001452 (Houston, TX: NACE, 2011).
5. F. Farelas, Y.S. Choi, S. Nesic, "Corrosion Behavior of API 5L X65 Carbon Steel Under Supercritical and Liquid Carbon Dioxide Phases in the Presence of Water and Sulfur Dioxide," *Corrosion* 69 (2013): p. 243.
6. Y.S. Choi, S. Nesic, "Effect of Water Content on the Corrosion Behavior of Carbon Steel in Supercritical CO_2 Phase with Impurities," CORROSION 2011, paper no. 11377 (Houston, TX: NACE, 2011).
7. Y.S. Choi, S. Hassani, T. N. Vu, S. Nesic, A.Z.B. Abas, "Effect of H_2S on the Corrosion Behavior of Pipeline Steels in Supercritical and Liquid CO_2 Environments," *Corrosion* 72 (2016): p. 999.
8. C. Sun, J. Sun, S. Liu, Y. Wang, "Effect of Water Content on the Corrosion Behavior of X65 Pipeline Steel in Supercritical CO_2-H_2O-O_2-H_2S-SO_2 Environment as Relevant to CCS Application," *Corrosion Science* 137 (2018): p. 151.
9. B.H. Morland, M. Tjelta, A. Dugstad, G. Svenningsen, "Corrosion in CO_2 Systems with Impurities Creating Strong Acids," *Corrosion* 75 (2019): p. 1307.
10. B.H. Morland, T. Norby, M. Tjelta, G. Svenningsen, "Effect of SO_2, O_2, NO_2, and H_2O Concentrations on Chemical Reactions and Corrosion of Carbon Steel in Dense Phase CO_2," *Corrosion* 75 (2019): p. 1327.
11. B.H. Morland, A. Dugstad, G. Svennigsen, "Experimental Based CO_2 Transport Specification Ensuring Material Integrity," Proceedings of the 15th Greenhouse Gas Control Technologies Conference 15-18 March 2021.
12. S. Hurter, D. Labregere, J. Berge, A. Desitter, "Impact of Mutual Solubility of H_2O and CO_2 on Injection Operations for Geological Storage of CO_2," ICPWS XV, Berlin, September 8-11, 2008.
13. M. Ahmad, S. Gersen, "Water Solubility in CO_2 Mixtures: Experimental and Modelling Investigation," *Energy Procedia* 63 (2014): p. 2402.
14. I. S. Cole, P. Corrigan, S. Sim, N. Birbilis, "Corrosion of Pipelines Used for CO_2 Transport in CCS: Is It a Real Problem?" *International Journal of Greenhouse Gas Control* 5 (2011): p. 749.
15. A. Dugstad, M. Halseid, B. Morland, A. O. Sivertsen, Corrosion in Dense Phase CO_2 – the Impact of Depressurization and Accumulation of Impurities," *Energy Procedia* 37 (2013): p. 3057.
16. I. S. Cole, W. D. Ganther, J. D. Sinclair, D. Lau, D. A. Paterson, "A Study of the Wetting of Metal Surfaces in Order to Understand the Processes Controlling Atmospheric Corrosion," *Journal of The Electrochemical Society*, 151 (2004): p. B627.
17. B.H. Morland, A. Tadesse, G. Svenningsen, R.D. Springer, A. Anderko, "Nitric and Sulfuric Acid Solubility in Dense Phase CO_2," *Ind. Eng. Chem. Res.* 58 (2019): p. 22924.
18. Y. Zhang, X. Pang, S. Qu, X. Li, K. Gao, "Discussion of the CO_2 Corrosion Mechanism Between Low Partial Pressure and Supercritical Condition," *Corrosion Science* 59 (2012): p. 186.

19. S. K. Vashist, P. Vashist, “Recent Advances in Quartz Crystal Microbalance-Based Sensors,” *Journal of Sensors* (2011): p. 571405.
20. M. D. Levi, G. Salitra, N. Levy, D. Aurbach, J. Maier, “Application of a Quartz-Crystal Microbalance to Measure Ionic Fluxes in Microporous Carbons for Energy Storage,” *Nature Materials* 8 (2009): p. 872.
21. A. Janshoff, C. Steinem, “Piezoelectric Sensors,” in Springer Series on Chemical Sensors and Biosensors, Vol. 5 (2007): p. 111-149.
22. A. Wexler, “Vapor Pressure Formulation for Water in Range 0 to 100°C: A Revision,” *Journal of Research of the National Bureau of Standards — A. Physics and Chemistry* 80A (1976): p. 775.
23. D. Sulzle, M. Verhoeven, J. K. Terlouw, H. Schwarz, “Generation and Characterization of Sulfurous Acid (H_2SO_3) and of Its Radical Cation as Stable Species in the Gas Phase,” *Angewandte Chem. Int. Ed. Engl.* 27 (1988): p.1533.
24. C. R. Bryan, T. A. Dewers, J. E. Heath, Y. Wang, E. N. Matteo, S. P. Meserole, D. R. Tallant, “Fundamental Study of CO_2-H_2O-Mineral Interactions for Carbon Sequestration, with Emphasis on the Nature of the Supercritical Fluid-Mineral Interface,” SANDIA REPORT, SAND2013-8251, Sandia National Laboratories.
25. C. Leygraf, I.O. Wallinder, J. Tidblad, T. Graedel, *Atmospheric Corrosion*, 2nd ed. (Hoboken, NJ: John Wiley & Sons, Inc., 2016), p. 27.
26. A. Poynor, L. Hong, I. K. Robinson, S. Granick, Z. Zhang, P. A. Fenter, “How Water Meets a Hydrophobic Surface,” *Physical Review Letters* 97 (2006): p. 266101.
27. S. Lee, R. W. Staehle, “Adsorption of Water on Copper, Nickle, and Iron,” *Corrosion* 53 (1997): p. 33.
28. Y. H. Kiang, “Predicting Dew points of Gases,” *Chemical Engineering* 88 (1981): p. 127.
29. W.M.M. Huijbregts, R. Leferink, “Latest Advances in the Understanding of Acid Dewpoint Corrosion: Corrosion and Stress Corrosion Cracking in Combustion Gas Condensates,” *Anti-Corrosion Methods and Materials*, 5 (2004): p. 173.